SPACE–TIME FINITE ELEMENT METHODS FOR SURFACE DIFFUSION WITH APPLICATIONS TO THE THEORY OF THE STABILITY OF CYLINDERS*

BERNARD D. COLEMAN[†], RICHARD S. FALK[†], AND MAHER MOAKHER[†]

Abstract. A family of space–time finite element approximation schemes is presented for the nonlinear partial differential equations governing diffusion in the surface of a body of revolution. The schemes share with the partial differential equations properties of conservation of volume and decrease of area. Numerical experiments are described showing that the result of the linear theory of small amplitude longitudinal perturbations of a cylinder to the effect that a long cylinder is stable against all perturbations with spatial Fourier spectra containing only wavelengths less than the circumference of the cylinder does not hold in the full nonlinear theory. Examples are given of cases in which longitudinal perturbations with high wave-number spectra grow in amplitude, after an initial rapid decay followed by a long "incubation period," and result in break-up of the body into a necklace of beads. The results of finite element calculations are compared with the predictions of a perturbation analysis.

Key words. axially symmetric motion by Laplacian of mean curvature, stability against surface diffusion

AMS subject classifications. 65M60, 73V05, 73T05

1. Introduction. We are concerned here with the numerical computation of morphological changes induced in an isotropic and homogeneous solid body by mass diffusion within the body's bounding surface S. We employ a constitutive equation, due to Herring [6], expressing the mass flux q in S as a linear function of the gradient in S of the sum H of the principal curvatures:

$$(1.1) \qquad q = -K\nabla_s H.$$

Here $K > 0$ is a material constant proportional to the surface self-diffusion coefficient of the isotropic material of which the body is composed, and we are using a sign convention for curvature such that H is positive for a sphere. As was observed and exploited by Mullins [9], when the only motion is the flux q in S, the mass balance yields the following relation between the rate v of advance of S along its exterior normal and the surface divergence of q:

$$(1.2) \qquad \rho v + \text{div}_s q = 0;$$

here ρ is the mass density, per unit volume, of the material in the body.

For a given characteristic length L, the theory of (1.1), (1.2) is rendered dimensionless by replacing quantities x, r, etc., with dimension of length by xL, rL, etc., the time t by $\rho L^4 t/K$, and hence q by Kq/L^2 and H by H/L. When this is done, (1.1), (1.2) yield

$$(1.3) \qquad v = \Delta_s H,$$

and thus are said to govern the theory of *motion by Laplacian of mean curvature*. That theory has a less-developed literature than the theory of *motion by mean curvature*, which is based on the equation

$$(1.4) \qquad v = -H.$$

In a recent survey [1], Cahn and Taylor discuss the difficulties encountered when one attempts to extend techniques employed to develop the theory of motion by mean curvature to the theory of motion by Laplacian of mean curvature. Whereas H in (1.4) is given by second-order spatial derivatives of surface coordinates, $\Delta_s H$ in (1.3) depends on fourth-order derivatives of the coordinates, and this elementary fact has the important consequence that a maximum principle employed in the theory of (1.4) does not hold for (1.3).

Among the papers presenting computational methods for motion by mean curvature are that of Dziuk [3], giving a semidiscretization scheme based on tangential gradients, and that of Sethian [11], based on a level set formulation of equation (1.4).

Among recent analytical developments in the analysis of the motion of surfaces by mean curvature are Huisken's short-time existence and regularity results [8], Soner and Songanidis's analysis of the nature of singularities in axially symmetric surfaces [12], and Evans and Spruck's theory of viscosity solutions [5] for a level set formulation of (1.4).

Interesting and very recent results in the theory of motion by Laplacian of mean curvature in a plane are proofs by Elliott and Garcke [4] of the asymptotic stability of circles and of global existence of planar solutions with initial data in a neighborhood of a circle.

The numerical methods and results presented here are for initial-value problems arising in the theory of motion by Laplacian of mean curvature for axially symmetric surfaces subject to periodic boundary conditions. In §2 we give various forms taken by the system (1.1), (1.2) for such surfaces and discuss relevant laws of conservation of volume and decrease of area [2]. A variational formulation presented in §3 is discretized in §4 with space–time finite element schemes that yield analogues of the laws of conservation of volume and decrease of area that hold for (1.1), (1.2). Results of numerical experiments are presented in §5.

For an axially symmetric surface, in a natural cylindrical coordinate system with radial coordinate r and axial coordinate x, the equation (1.3) of motion by Laplacian of mean curvature becomes

$$(1.5) \qquad r_t = \frac{1}{r}\left[\frac{r}{(1+r_x^2)^{1/2}}\left(\frac{1}{r(1+r_x^2)^{1/2}} - \frac{r_{xx}}{(1+r_x^2)^{3/2}}\right)_x\right]_x.$$

The emphasis here is on cases in which this equation is subject to initial data of the form

$$(1.6) \qquad r(x,0) = r_0(x) = 1 + \epsilon u(x)$$

with $\epsilon > 0$ and u an almost periodic function. For simplicity we often take u to have a finite Fourier spectrum, i.e., to be of the form

$$(1.7) \qquad u(x) = \sum_{i=1}^{M} c_i \sin(k_i x + \varphi_i)$$

with c_i, $k_i > 0$. (In the numerical calculations of this paper u is assumed periodic and hence the wave numbers k_i in (1.7) are commensurate.) For longitudinal perturbations of a cylinder of radius a, (1.5) is obtained from (1.1), (1.2) by putting $L = a$ and making the change of units discussed above. For a given u, the perturbation is small if ϵ is small compared with 1, and, in (1.7), $k_i < 1$, $= 1$, or > 1, in accord with whether the corresponding period $P_i = 2\pi/k_i$ exceeds, equals, or is less than the circumference of the unperturbed cylinder.

Since the work of Nichols and Mullins [10], in the study of small amplitude longitudinal perturbations of a cylinder it has been customary to restrict attention to the linearization of (1.5) about $r = 1$, i.e., to the equation

$$(1.8) \qquad r_t + r_{xxxx} + r_{xx} = 0,$$

whose solution with the initial condition (1.6), (1.7) is

$$(1.9) \qquad r(x, t) = 1 + \epsilon \sum_{i=1}^{M} c_i e^{\alpha(k_i)t} \sin(k_i x + \varphi_i)$$

where α obeys the dispersion relation

$$(1.10) \qquad \alpha(k) = k^2(1 - k^2).$$

The maximum value of $\alpha(k)$ is $\frac{1}{4}$ and occurs at $k = 1/\sqrt{2}$. As the right side of (1.10) is negative for $k > 1$, the linear equation (1.8) implies that whenever, in (1.7), $k_i > 1$ for all i, the perturbation decays to zero as $t \to \infty$. We recently presented arguments [2] to the effect that such is not the case in the theory of the nonlinear equation (1.5).

The arguments given in [2] are based on formal perturbation analyses employing an expansion of the solution of (1.5), (1.6) in ϵ. A perturbation argument taking into account terms $O(\epsilon^2)$ yields the conclusion that if

$$(1.11a) \qquad k_i > 1 \qquad \text{for} \qquad i = 1, \ldots, M$$

and, in addition, two distinct wave numbers, k_i, k_j, have $|k_i - k_j| < 1$, then, although the solution of (1.5) will exhibit an initial decay of the perturbation, after a time whose duration can be estimated, a new sinusoidal term with wave number equal to $|k_i - k_j|$, i.e., to that of the envelope of the ith and jth terms in (1.7), will appear in the solution and grow in amplitude, taking the surface far from cylindrical shape. When terms $O(\epsilon^n)$ are taken into account the following generalization of this conclusion is obtained: if (1.11a) holds, and, in addition, there is an integer $n \geq 2$ and there are M integers m_i (positive, negative, or zero) that obey the relations

$$(1.11b) \qquad \sum_{i=1}^{M} |m_i| = n \qquad \text{and} \qquad 0 < \left| \sum_{i=1}^{M} m_i k_i \right| < 1,$$

then, again after an initial decay, the perturbation will grow.

The perturbation analysis given in [2] and discussed here in §5 leads one to expect, but cannot be employed to prove, that in the cases in which (1.11a) and (1.11b) hold the growth in perturbations proceeds until there is a time t^* and values x^* of x for which $\lim_{t \to t^*} r(x^*, t) = 0$. The numerical methods we present here were developed to see if such is the case and, if so, to permit precise calculation of the break-up time t^* as well as the "incubation time" required for occurrence of appreciable growth of a perturbation after its initial (and generally rapid) decay. Numerical experiments confirming expectations based on the perturbation analysis are described in §5. We also give there an example of a case in which our numerical methods can be applied to study the evolution of the body for $t > t^*$. In general, a topological change occurs at $t = t^*$, resulting in the break-up of the original body into separated subbodies. Thus we refer to t^* as the "time of break-up." (In the theory of motion by mean curvature, in which the volume is not conserved but decreases in time, similar phenomena can occur, and their times of occurrence are often referred to as times of "pinch-off.")

2. Basic equations. To describe the evolution of the surface of an infinite body of revolution, we continue to use the cylindrical coordinates x and r of equation (1.5). We write t for the unit tangent to the time-dependent curve $r = r(x, t)$ in the (x, r)-plane, and we define the signed magnitude q of $\boldsymbol{q}$ so that $\boldsymbol{q} = q\boldsymbol{t}$. For axially symmetric surfaces, when the

dimensionless units are used, (1.2) and (1.1) become, respectively,

$$(2.1) \qquad\qquad rr_t = -(rq)_x,$$

$$(2.2) \qquad\qquad q = -(\nabla_s H) \cdot t = -\frac{H_x}{\sqrt{1 + r_x^2}}$$

where

$$(2.3) \qquad\qquad H = \frac{1}{r}\left[\sqrt{1 + r_x^2} - \left(\frac{rr_x}{\sqrt{1 + r_x^2}}\right)_x\right].$$

For numerical calculations we treat the body as one with finite length subject to space-periodic boundary conditions with, say, period P. The resulting problems have properties of volume conservation and area decay which we now discuss.

It follows from (2.1) that the volume of material lying between cross-sectional planes $x = a$ and $x = b$ with $b - a = P$, i.e.,

$$(2.4) \qquad\qquad V(t) = \pi \int_a^b r^2 \, dx,$$

is constant in time if r and $q = -H_x/\sqrt{1 + r_x^2}$ are P-periodic. Equations (2.1) and (2.2) together imply that the surface area (or the free energy) of the portion of the body lying between these two planes, i.e.,

$$(2.5) \qquad\qquad \Psi(t) = 2\pi \int_a^b r\sqrt{1 + r_x^2} \, dx,$$

is a monotone-decreasing function of time, provided that not only r and $H_x/\sqrt{1 + r_x^2}$ but also H and $r_x/\sqrt{1 + r_x^2}$ are P-periodic. The periodicity of r, H, $r_x/\sqrt{1 + r_x^2}$, and $H_x/\sqrt{1 + r_x^2}$ are equivalent to the periodicity of r, H, r_x, and H_x. Thus, under boundary conditions implying such periodicity, V is preserved and Ψ represents a Lyapunov function for the evolution of r.

We put $\Omega = (a, b)$ and write $\mathcal{I} = (0, T)$ for an interval with $T > 0$ on which solutions of (2.1)–(2.3) with $r > 0$ are defined. Under the conditions of periodicity just described

$$(2.6) \qquad \dot{\Psi} = -2\pi \int_\Omega \frac{rH_x^2}{\sqrt{1 + r_x^2}} dx = -2\pi \int_\Omega q^2 r \sqrt{1 + r_x^2} dx \le 0,$$

and hence under the same conditions

$$(2.7) \qquad \Phi(t) = \Psi(t) + 2\pi \int_0^t \int_\Omega q^2(x, \tau) r(x, \tau)\sqrt{1 + r_x^2(x, \tau)} \, dx \, d\tau$$

is constant:

$$(2.8) \qquad\qquad \Phi(t) = \Phi(0) = \Psi(0).$$

For each initial configuration r_0 we seek $r(\cdot, t)$ satisfying (2.1), (2.2), and the periodicity conditions. The equation of evolution for r, (1.5), which is fourth order in the space variable x, can be formulated in terms of r and H to yield a coupled system of second order in x. The resulting fully nonlinear initial-value problem with periodic boundary conditions has a variational formulation that can be slightly simplified by introducing a function R defined by

$$(2.9) \qquad\qquad R(x, t) = \frac{1}{2}r^2(x, t).$$

In this way we are led to the following problem.

Problem RH. Find (R, H) with $R > 0$ satisfying

$$(2.10) \qquad R_t = \left(\frac{2RH_x}{\sqrt{2R + R_x^2}} \right)_x \qquad \forall (x, t) \in \Omega \times \mathcal{I},$$

$$(2.11) \qquad H = \frac{1}{\sqrt{2R + R_x^2}} - \left(\frac{R_x}{\sqrt{2R + R_x^2}} \right)_x \qquad \forall (x, t) \in \Omega \times \mathcal{I},$$

with the periodic boundary conditions

$$
R(a, t) = R(b, t), \qquad R_x(a, t) = R_x(b, t) \qquad \forall t \in \mathcal{I},
$$
$$(2.12) \qquad H(a, t) = H(b, t), \qquad H_x(a, t) = H_x(b, t) \qquad \forall t \in \mathcal{I},$$

and the initial condition

$$(2.13) \qquad R(x, 0) = R_0(x) = \frac{1}{2} r_0^2(x) \qquad \forall x \in \Omega.$$

3. Variational formulation. We use standard notation: $L^2(\Omega)$ is the space of square integrable functions on Ω, $L^\infty(\Omega)$ is the space of essentially bounded functions on Ω, $H^1(\Omega)$ is the Sobolev space of functions in $L^2(\Omega)$ with distributional derivative in $L^2(\Omega)$, and $W^{1,\infty}(\Omega)$ is the Sobolev space of functions in $L^\infty(\Omega)$ with distributional derivative in $L^\infty(\Omega)$. Of importance here are subspaces H_P^1 and $W_P^{1,\infty}$ of $H^1(\Omega)$ and $W^{1,\infty}(\Omega)$, with $\Omega = (a, b)$, that arise from our concern with periodic boundary conditions

$$H_P^1 = \left\{ v \in H^1(\Omega) : v(a) = v(b) \right\},$$

$$W_P^{1,\infty} = \left\{ v \in W^{1,\infty}(\Omega) : v(a) = v(b) \right\}.$$

We also define H_P^{-1} as the dual space of H_P^1. Let X be a Banach space on Ω with norm $\| \cdot \|_X$. We denote by $L^2(0, T; X)$ the space of functions f from $(0, T)$ into X such that $(\int_0^T \| f \|_X^2 dt)^{1/2} < \infty$ and by $L^\infty(0, T; X)$ the space of functions f from $(0, T)$ into X such that $\| f \|_X$ is essentially bounded on $(0, T)$.

For brevity we write

$$(f, g) = \int_\Omega fg \, dx.$$

Variational form of Problem RH. Find $R \in L^\infty(0, T; W_P^{1,\infty})$ with $R > 0$ and $R_t \in L^2(0, T; H_P^{-1})$ and $H \in L^2(0, T; H_P^1)$ satisfying

$$(3.1) \qquad \int_0^T (R_t, u) \, dt + \int_0^T \left(\frac{2RH_x}{\sqrt{2R + R_x^2}}, u_x \right) dt = 0 \quad \forall u \in L^2(0, T; H_P^1),$$

$$(3.2) \qquad \int_0^T (H, v) \, dt = \int_0^T \left(\frac{1}{\sqrt{2R + R_x^2}}, v \right) dt + \int_0^T \left(\frac{R_x}{\sqrt{2R + R_x^2}}, v_x \right) dt \quad \forall v \in L^2(0, T; H_P^1),$$

$$(3.3) \qquad (R(\cdot, 0), w) = (R_0, w) \quad \forall w \in L^2(\Omega).$$

We note that there are not yet available proofs of existence and uniqueness for solutions for either Problem RH or (3.1)–(3.3). However, if we are granted existence and uniqueness, the stated variational form of Problem RH is a useful formulation for the construction of the conforming finite element approximation schemes presented in §4.

Straightforward arguments show that solutions of (2.10)–(2.13) obey (3.1)–(3.3) and that solutions of the variational equations (3.1)–(3.3) with sufficient regularity obey (2.10)–(2.13).

Constancy of volume and monotone decrease of surface area hold for each solution (R, H) of (3.1)–(3.3). To show this, we observe that in our present notation

$$\dot{V} = 2\pi(R_t, 1), \tag{3.4}$$

and hence by putting $u \equiv 1$ in the time interval $(0, t)$ and $u \equiv 0$ in the time interval (t, T) in equation (3.1), we obtain

$$V(t) = V(0). \tag{3.5}$$

In (3.1) and (3.2) by putting $u = H$ and $v = R_t$ in the time interval $(0, t)$ and $u \equiv 0$, $v \equiv 0$ in the time interval (t, T), both of which are admissible test functions, we obtain

$$\int_0^t (R_t, H)\, dt + \int_0^t \left(\frac{2R}{\sqrt{2R + R_x^2}}, H_x^2 \right) dt = 0, \tag{3.6}$$

$$\int_0^t (H, R_t)\, dt = \int_0^t \left(\frac{1}{\sqrt{2R + R_x^2}}, R_t \right) dt + \int_0^t \left(\frac{R_x}{\sqrt{2R + R_x^2}}, R_{tx} \right) dt. \tag{3.7}$$

As $\Psi = 2\pi(\sqrt{2R + R_x^2}, 1)$ and hence

$$\dot{\Psi} = 2\pi \left(\frac{1}{\sqrt{2R + R_x^2}}, R_t \right) + 2\pi \left(\frac{R_x}{\sqrt{2R + R_x^2}}, R_{tx} \right), \tag{3.8}$$

(3.7) yields $\int_0^t \dot{\Psi}\, dt = 2\pi \int_0^t (H, R_t)\, dt$, and, by (3.6),

$$\Psi(t) - \Psi(0) = -2\pi \int_0^t \left(\frac{2R}{\sqrt{2R + R_x^2}}, H_x^2 \right) dt. \tag{3.9}$$

Hence

$$\Psi(t) - \Psi(0) = -2\pi \int_0^t \left(\frac{2R}{\sqrt{2R + R_x^2}}, H_x^2 \right) dt \leq 0.$$

4. Finite element method. To approximate the variational form of Problem RH, we here construct a family of mixed finite element methods for which piecewise polynomial approximations in space and time are used for both R and H. Let $a = x_0 < x_1 < \cdots < x_N = b$ and $0 = t^0 < t^1 < \cdots < t^K = T$ be partitions of Ω and $\mathcal{I}$, and let $h_i = x_{i+1} - x_i$, $i = 0, \ldots, N - 1$ and $k^j = t^{j+1} - t^j$, $j = 0, \ldots, K - 1$, be mesh spacings and time steps. Let $S_h^p(\Omega)$ be the finite element space of continuous functions Q that are piecewise polynomials of degree $p \geq 1$ on each interval of the partition of Ω and obey the periodicity condition $Q(a) = Q(b)$. We write $S_k^q(\mathcal{I})$ and $\bar{S}_k^q(\mathcal{I})$, respectively, for the finite element spaces of continuous and discontinuous functions that are piecewise polynomials of degree $q \geq 0$ on each interval of the partition of $\mathcal{I}$. The members of the tensor product spaces

$$S_{hk}^{p,q} = S_h^p(\Omega) \otimes S_k^q(\mathcal{I}), \qquad \bar{S}_{hk}^{p,q} = S_h^p(\Omega) \otimes \bar{S}_k^q(\mathcal{I})$$

are functions on $\Omega \times \mathcal{I}$. We consider, for given integers $p \geq 1$, $q \geq 0$, the following.

Finite element approximation of type (p, q) to Problem RH. Find $R_{hk} \in S_{hk}^{p,q+1}$ and $H_{hk} \in \bar{S}_{hk}^{p,q}$ satisfying

$$\int_0^T ((R_{hk})_t, u_{hk})dt + \int_0^T \left(\frac{2R_{hk}(H_{hk})_x}{\sqrt{2R_{hk} + (R_{hk})_x^2}}, (u_{hk})_x \right) dt = 0 \qquad \forall u_{hk} \in \bar{S}_{hk}^{p,q},$$

$$\int_0^T (H_{hk}, v_{hk})dt = \int_0^T \left(\frac{(R_{hk})_x}{\sqrt{2R_{hk} + (R_{hk})_x^2}}, (v_{hk})_x \right) dt$$

$$+ \int_0^T \left(\frac{1}{\sqrt{2R_{hk} + (R_{hk})_x^2}}, v_{hk} \right) dt \qquad \forall v_{hk} \in \bar{S}_{hk}^{p,q},$$

$$(R_{hk}(\cdot, 0), w_{hk}) = (R_0, w_{hk}) \qquad \forall w_{hk} \in S_h^p(\Omega).$$

We note that R_{hk} is a polynomial of one degree higher in time than H_{hk} and the test functions u_{hk} and v_{hk}. The simplest finite element approximation in this family is that of type (p, q) with $p = 1$ and $q = 0$, i.e., that for which R_{hk} is a continuous piecewise linear polynomial in both space and time and H_{hk} and the test functions u_{hk} and v_{hk} are continuous piecewise linear polynomials in space and piecewise constant in time.

Because the test functions u_{hk} and v_{hk} are discontinuous in time, finite element solutions (R_{hk}, H_{hk}) can be computed by marching through successive time intervals. Let $P^q(\mathcal{I}^n)$ be the set of polynomials on $\mathcal{I}^n = [t^n, t^{n+1}]$ of degree q. On the time-strip $\mathcal{I}^n$ the appropriate restrictions of R_{hk} and H_{hk} belong to $S_h^p(\Omega) \otimes P^{q+1}(\mathcal{I}^n)$ and $S_h^p(\Omega) \otimes P^q(\mathcal{I}^n)$, respectively, and obey, for each u_{hk} and v_{hk} in $S_h^p(\Omega) \otimes P^q(\mathcal{I}^n)$,

(4.1) $$\int_{t^n}^{t^{n+1}} ((R_{hk})_t, u_{hk})dt + \int_{t^n}^{t^{n+1}} \left(\frac{2R_{hk}(H_{hk})_x}{\sqrt{2R_{hk} + (R_{hk})_x^2}}, (u_{hk})_x \right) dt = 0,$$

$$\int_{t^n}^{t^{n+1}} (H_{hk}, v_{hk})dt = \int_{t^n}^{t^{n+1}} \left(\frac{(R_{hk})_x}{\sqrt{2R_{hk} + (R_{hk})_x^2}}, (v_{hk})_x \right) dt$$

(4.2)

$$+ \int_{t^n}^{t^{n+1}} \left(\frac{1}{\sqrt{2R_{hk} + (R_{hk})_x^2}}, v_{hk} \right) dt$$

where R_{hk} at $t = t^n$ is fixed by continuity (or by the initial condition if $n = 0$).

The arguments which gave us (3.4) and (3.8) hold for the spaces to which R_{hk}, H_{hk}, u_{hk}, and v_{hk} belong for each finite element approximation, and each approximate solution (R_{hk}, H_{hk}) will show constancy of V and Φ and monotone decrease of Ψ.

In the simplest case, $p = 1$ and $q = 0$, we write $R_{hk}(x, t)$ on the time-strip $\mathcal{I}^n$ as

$$R_{hk}(x, t) = \frac{t - t^n}{k^n}[R_{hk}(x, t^{n+1}) - R_{hk}(x, t^n)] + R_{hk}(x, t^n),$$

and $H_{hk}(x, t)$ reduces to the constant-in-time function $H_{hk}(x, t) = H_{hk}(x, (t^n + t^{n+1})/2)$. Upon use of the usual expansion in piecewise linear basis functions, (4.1) and (4.2) yield a system of nonlinear algebraic equations for the coefficients of the basis functions. In our numerical work that algebraic system was solved by an iteration procedure which was initialized with the choice $R_{hk}^0(x, t^1) = R_{hk}(x, t^0)$ for the time-strip $\mathcal{I}^0 = [t^0, t^1]$ and carried forward

with the extrapolation

$$R_{hk}^0(x, t^{n+1}) = \left(1 + \frac{k^n}{k^{n-1}}\right) R_{hk}(x, t^n) - \frac{k^n}{k^{n-1}} R_{hk}(x, t^{n-1})$$

for the strip $\mathcal{I}^n$, $n \geq 1$; here R_{hk}^l denotes the lth iterate of R_{hk}. At the lth iteration on $\mathcal{I}^n$, $n \geq 0$, R_{hk}^l, and H_{hk}^l are determined by solving the linear system

$$\int_{t^n}^{t^{n+1}} ((R_{hk}^l)_t, u_{hk}) dt + \int_{t^n}^{t^{n+1}} \left(\frac{2R_{hk}^{l-1}(H_{hk}^l)_x}{\sqrt{2R_{hk}^{l-1} + (R_{hk}^{l-1})_x^2}}, (u_{hk})_x\right) dt = 0,$$

$$\int_{t^n}^{t^{n+1}} (H_{hk}^l, v_{hk}) dt = \int_{t^n}^{t^{n+1}} \left(\frac{(R_{hk}^l)_x}{\sqrt{2R_{hk}^{l-1} + (R_{hk}^{l-1})_x^2}}, (v_{hk})_x\right) dt$$

$$+ \int_{t^n}^{t^{n+1}} \left(\frac{1}{\sqrt{2R_{hk}^{l-1} + (R_{hk}^{l-1})_x^2}}, v_{hk}\right) dt$$

with u_{hk} and v_{hk} as in (4.1), (4.2) and

$$R_{hk}^l(x, t) = \frac{t - t^n}{k^n}[R_{hk}^l(x, t^{n+1}) - R_{hk}(x, t^n)] + R_{hk}(x, t^n).$$

5. Numerical experiments. For the two numerical experiments described below, we employed a finite element approximation of type $(1, 0)$. The initial data had the form (1.6), (1.7) with each phase angle, φ_i, zero and, more importantly, each wave-number k_i greater than 1, so that (1.10) yields

$$(5.1) \qquad \alpha(k_i) < 0, \qquad i = 1, \ldots, M,$$

and hence each exponential term in the solution (1.9) of the linear equation (1.8) decays to zero. The wave-numbers k_i were taken to be commensurate, which makes the periodic boundary conditions (2.12) exact relations.

Let $\bar{r}$ be given by

$$(5.2) \qquad \pi(b - a)\bar{r}^2 = V(0) = \pi \int_a^b r_0^2 dx$$

and put

$$(5.3) \qquad g(t) = \sup_x |r(x, t) - \bar{r}|.$$

A cylindrical body can be said to be *asymptotically stable against a class $\mathcal{P}$ of perturbations*, ϵu, if for each function $r_0 = 1 + \epsilon u$ with ϵu in $\mathcal{P}$ the solution of Problem RH obeys the two conditions

$$(I) \qquad r(x, t) > 0 \qquad \forall (x, t) \in \Omega \times (0, \infty)$$

and

$$(II) \qquad g(t) \to 0 \qquad \text{as} \qquad t \to \infty.$$

(I) asserts that "break-up" does not occur; (II) asserts that in the limit as $t \to \infty$ the body returns to cylindrical shape with a radius $\bar{r}$ determined by the mean volume $V(0)/(b - a)$ of the perturbed cylinder. (To generalize the condition (II) to initial data that are not periodic, but instead, say, almost periodic, one may replace $V(0)/(b - a)$ in the definition of $\bar{r}$ by the

quantity

$$(5.4) \qquad \langle \pi r^2 \rangle = 2 \langle \pi R \rangle = \lim_{X \to \infty} \frac{\pi}{2X} \int_{-X+x_0}^{X+x_0} r^2 dx$$

which is constant in time and, for almost periodic functions, independent of x_0.)

When the function u in (1.6) is specified, the solution r of the nonlinear equation (1.5) depends on ϵ. For the perturbation analysis given in [2] we made the usual assumption that the dependence of $r(x, t; \epsilon)$ on ϵ is sufficiently smooth that for each integer n one can write

$$(5.5) \qquad r(x, t; \epsilon) = 1 + \sum_{l=1}^{n} \epsilon^l w^{(l)}(x, t) + O(\epsilon^{n+1}).$$

By placing (5.5) in (1.5) and using (1.6) with u as in (1.7) we found, using a perturbation analysis of order 2, i.e., setting $n = 2$ in (5.5), that the term $1 + \epsilon w^{(1)}(x, t)$ is given by the right-hand side of (1.9), and

$$(5.6) \qquad w^{(2)}(x, t) = \frac{1}{4} \sum_{i=1}^{M} c_i^2 - \frac{1}{4} \sum_{i=1}^{M} c_i^2 e^{2\alpha(k_i)t} + \sum_{i=1}^{M} A_1(i; t) \cos(2k_i x + 2\varphi_i)$$

$$+ \sum_{1 \le i < j \le M} A_2(i, j; t) \cos((k_i + k_j)x + \varphi_i + \varphi_j)$$

$$+ \sum_{1 \le i < j \le M} A_3(i, j; t) \cos((k_i - k_j)x + \varphi_i - \varphi_j)$$

where

$$(5.7a) \qquad A_1(i; t) = \frac{3c_i^2 \beta(k_i)}{2[\alpha(2k_i) - 2\alpha(k_i)]} (e^{\alpha(2k_i)t} - e^{2\alpha(k_i)t}),$$

$$(5.7b) \qquad A_2(i, j; t) = \frac{c_i c_j \beta^+(k_i, k_j)}{\alpha(k_i + k_j) - \alpha(k_i) - \alpha(k_j)} (e^{\alpha(k_i+k_j)t} - e^{(\alpha(k_i)+\alpha(k_j))t}),$$

$$(5.7c) \qquad A_3(i, j; t) = \frac{c_i c_j \beta^-(k_i, k_j)}{\alpha(k_i - k_j) - \alpha(k_i) - \alpha(k_j)} (e^{\alpha(k_i-k_j)t} - e^{(\alpha(k_i)+\alpha(k_j))t})$$

with α as in (1.10) and

$$(5.8a) \qquad \beta(k) = k^2(1 + k^2),$$

$$(5.8b) \qquad \beta^+(k_i, k_j) = (k_i k_j + k_i^2 + k_j^2)(1 + k_i k_j),$$

$$(5.8c) \qquad \beta^-(k_i, k_j) = (k_i k_j - k_i^2 - k_j^2)(1 - k_i k_j).$$

When, as in the numerical experiments, (1.11a) holds, the quantities $\alpha(k_i)$, $\alpha(2k_i)$, $\alpha(k_i + k_j)$ are negative for each i and $j > i$. Hence not only $w^{(1)}$ but also all the terms in $w^{(2)}$, other than the constant term $\frac{1}{4}\epsilon^2 \sum_{i=1}^{M} c_i^2$ and possibly some of the form $\epsilon^2 f(k_i, k_j; t) \cos((k_i - k_j)x + \varphi_i - \varphi_j)$ with

$$(5.9) \qquad f(k_i, k_j; t) = \frac{c_i c_j \beta^-(k_i, k_j)}{\alpha(k_i - k_j) - \alpha(k_i) - \alpha(k_j)} e^{\alpha(k_i-k_j)t},$$

will decay to zero exponentially with increasing t. The quantity $|f(k_i, k_j; t)|$ is constant in time when $|k_i - k_j| = 1$; it increases exponentially if and only if

$$(5.10) \qquad\qquad 0 < |k_i - k_j| < 1.$$

Thus, if (1.11a) holds and in addition $|k_i - k_j| > 1$ for all distinct pairs (i, j), the second-order perturbation analysis, like the linear theory, does not yield the existence of times at which $g(t)$ increases; however, a higher analysis may yield such times. In fact, exponential growth of $g(t)$, beginning at some time $t > 0$ and proceeding until break-up occurs, i.e., until a time t^* at which there are values x^* of x with $r(x^*, t^*) = 0$, will be shown in an nth-order perturbation analysis if (1.11b) holds for an M-tuple $(m_1, m_2, \ldots, m_M)$ with the m_i having (positive, negative, or zero) integral values.

In the numerical experiments reported here (1.11a) and (5.10) hold for at least one pair (i, j), $i < j$, and hence although the linear theory based on (1.8) predicts that the cylindrical body is asymptotically stable against the perturbation studied, the second-order theory predicts that the body is not stable against the perturbation and suggests that break-up can occur at a finite time. Specifically, under the conditions of the experiments, the second-order analysis yields the conclusion that for short times $r(x, t)$ is approximated by the expression

$$1 + \frac{\epsilon^2}{4} \sum_{i=1}^{M} c_i^2 + \epsilon \sum_{i=1}^{M} c_i e^{\alpha(k_i)t} \sin(k_i x + \varphi_i)$$

where each $\alpha(k_i)$ is negative, and hence, after a brief time interval, $r(x, t)$ will be close for all x to the constant

$$\bar{r} = \left[1 + \frac{\epsilon^2}{2} \sum_{i=1}^{M} c_i^2 \right]^{1/2} = 1 + \frac{\epsilon^2}{4} \sum_{i=1}^{M} c_i^2 + O(\epsilon^4);$$

i.e., the body will be essentially indistinguishable from a cylinder. In a subsequent time interval, however, $r(x, t)$ will be approximated by

$$1 + \frac{\epsilon^2}{4} \sum_{i=1}^{M} c_i^2 + \epsilon^2 \sum_{(i,j) \in \Gamma} f(k_i, k_j; t) \cos((k_i - k_j)x + \varphi_i - \varphi_j)$$

where f is as in (5.9) and Γ is the set of pairs (i, j) with $1 \le i < j \le M$ and $|k_i - k_j| < 1$; during that interval $g(t)$ will increase monotonically.

Let ν be the minimum value that $g(t)$ must have for a departure of the body from cylindrical shape to be easily observable after $g(t)$ has decayed and started to increase. The time $t_\#$ at which $g(t)$ attains the value ν (after an initial decrease) may be called the "incubation time" for observable growth of a perturbation which according to the linear theory (1.8) would only decay. The second-order perturbation analysis gives the following relation for $t_\#$ in the case in which there is precisely one pair (i, j) for which (5.10) holds:

$$(5.11) \qquad\qquad \nu = \epsilon^2 f(k_i, k_j; t_\#).$$

A reasonable value for ν would be 0.05. We note that equation (5.11) implies that $t_\#$ varies slowly, i.e., logarithmically, with ϵ.

For large k, $\alpha(k)$ decreases rapidly with k; indeed, as $\alpha(k) \sim -k^4$. However, on the interval $0 < k < 1$ where $\alpha(k)$ is positive, the maximum value of $\alpha(k)$, $\alpha(1/\sqrt{2})$, is only $\frac{1}{4}$. Hence the incubation time $t_\#$ can be expected to be orders of magnitude longer than the

time required for decay of an initial perturbation that has each k_i appreciably greater than 1. This disparity in time scales requires that time steps be adjusted in numerical calculations in accord with the rate of convergence of the iterative procedure described at the end of §4, i.e., in accord with the rate of evolution of R and H.

For the first numerical experiment the initial data correspond to the function

$$(5.12) \qquad r_0(x) = 1 + 5 \times 10^{-2} \left[\sin(5x) + \sin(11x/2) \right],$$

which has minimum period 4π. Here $k_1 = 5 > 1$, $k_2 = 11/2 > 1$, but $|k_1 - k_2| = 1/2 < 1$. According to the second-order perturbation analysis, the two sinusoidal terms in the initial data should decay rapidly, and, after this rapid decay, which in the present case lasts until approximately $t = 2 \times 10^{-2}$, $r(x,t)$ should be, for a while, close to a cosine function of x which has period 4π and an amplitude growing as $e^{\alpha(1/2)t}$ with $\alpha(1/2) = 3/16$. In the finite element scheme, the interval $a \leq x \leq b$ was chosen to have length 8π, i.e., two periods, and was discretized into 512 equal segments. For the time interval $0 < t \leq 5 \times 10^{-2}$ that contains the times of rapid decay of $g(t)$, the time step, Δt, was chosen to be 10^{-4}; during the early growth phase, i.e., for $5 \times 10^{-2} < t \leq 28.05$, Δt was set equal to $t = 10^{-2}$. For $28.05 \leq t \leq 28.27234 = t^*$, the time steps were refined in such a way that Δt decreased rapidly as t approached the break-up time t^*. (As is common practice, we repeated suspected critical parts of this and the second numerical experiment using refined spatial and temporal meshes; the reported mesh densities are such that further refinement produced no change in results.)

In Fig. 1 there are graphs of r versus x for various t between 0 and t^*. The initial data, (5.12), are shown in Fig. 1a. The scale of the ordinate r contracts in the sequence from Fig. 1b to Fig. 1f, but in each case is greater than that of the abscissa x. Figure 1b contains graphs corresponding to $t = 10^{-2}$ and $t = 1.63 \times 10^{-2}$. At $t = 10^{-2}$ remnants of the terms $5 \times 10^{-2} \sin(5x)$ and $5 \times 10^{-2} \sin(11x/2)$ can be seen perturbing the function $\tilde{r}(\cdot, t)$ given by

$$(5.13) \qquad \tilde{r}(x,t) = \bar{r} + \epsilon^2 f(5, 11/2; t) \cos(x/2)$$

where $\epsilon^2 = 25 \times 10^{-4}$ and f is as in (5.9) with $\alpha = 3/16$. At $t = 1.63 \times 10^{-2}$, $g(t)$ attains its minimum value, and at that time the difference between $r(x,t)$ and $\tilde{r}(x,t)$ is not detectable on the scale employed for r of Fig. 1b. Figure 1c contains graphs for values of t at which $r(x,t)$ is close to $\tilde{r}(x,t)$; the earliest time at which the second-order perturbation analysis gives results (here plotted with dashes) that are distinguishable from the finite element results (on the scale of Fig. 1c) is $t = 15$.

In Fig. 2, where we employ equal scales for the ordinate and the abscissa, there are shown profiles of the axially symmetric body whose surface is given by $r = r(x,t)$. The initial configuration is seen in Fig. 2a. At a time $t \sim 10^{-2}$ the body is of cylindrical shape to within an error of the order 0.1% in r. If we set $\nu = 0.05$, the configuration shown in Fig. 2b, i.e., that for $t = 20$, is very close to one with $g(t) = \nu$; in fact, the finite element results yield 0.05 for $g(t)$ when $t = 19.55$; the second-order perturbation analysis, on the other hand, yields 0.05 for $g(t)$ when $t = 19.72$. We think it remarkably fortunate that in this case an elementary analysis that takes into account only the lowest-order nonlinear terms gives an estimate for the incubation time $t_\#$ that is off by only 1%.

There are cases in which the evolution of the subbodies formed at time t^* can be studied for $t > t^*$ by reparameterizing with spherical coordinates the surface of each connected subbody. In this procedure one chooses a point on the original x-axis to be the origin of a spherical coordinate system, and the closed surface of the subbody containing that origin is described by giving the distance $\hat{r}$ from the origin to a point on the surface as a function of t and the colatitude φ measured from the x-axis. A finite element method analogous to
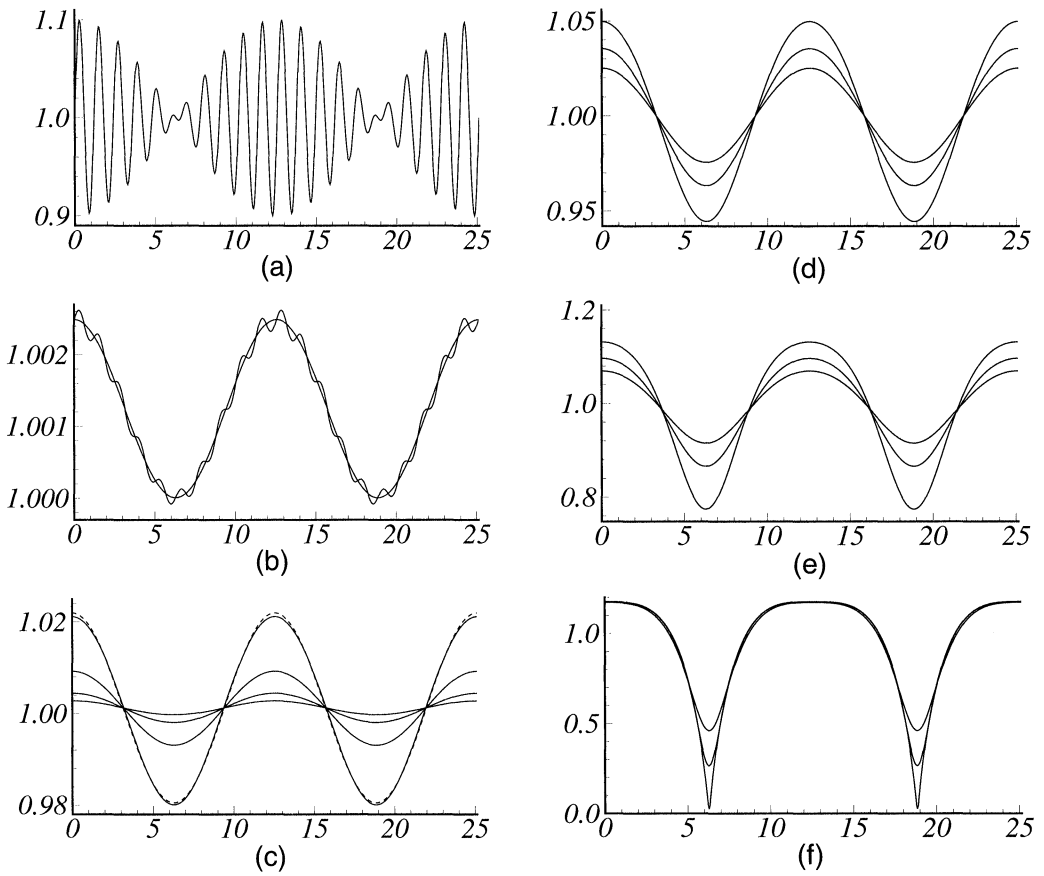
FIG. 1. *The radius r as a function of x at various times t in the first numerical experiment:* (a) $t = 0$; (b) $t = 10^{-2}$ *(wavy line),* $t = 1.63 \times 10^{-2}$; (c) $t = 0.1, 5, 10, 15$ *(the dashed curve gives the result of the second-order perturbation analysis at $t = 15$);* (d) $t = 16, 18, 20$; (e) $t = 22, 24, 26$; (f) $t = 28, 28.25, 28.27234$.
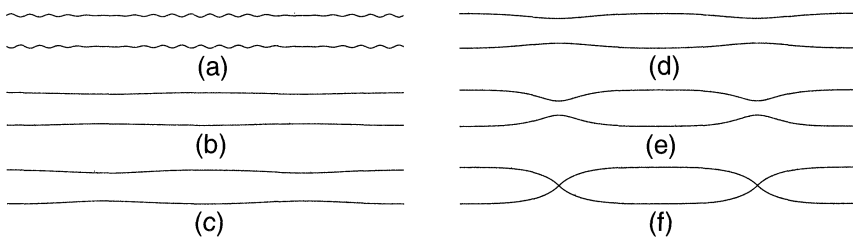

FIG. 2. *Profiles at selected times in the first experiment:* (a) $t = 0$; (b) $t = 20$; (c) $t = 23$; (d) $t = 25.5$; (e) $t = 28$; (f) $t = t^* = 28.27234$.

that employed for the cylindrical-coordinate formulation gives satisfactory results in cases in which, for *all* $t > t^*$, the closed surface remains star shaped with respect to a fixed point. We note that for motion by Laplacian of mean curvature there is no analogue of Huisken's theorem [7] in the theory of motion by mean curvature, asserting that if a closed surface deforming in accord with (1.4) is convex at one time t^0 then it is convex at all subsequent times.
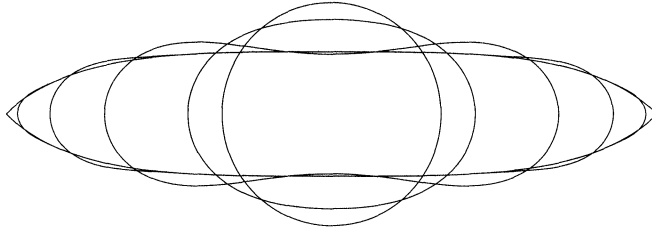
FIG. 3. *Profiles in the first experiment at times* $t = t^* + \hat{t}$ *for* $\hat{t} = 0, 10^{-3}, 10^{-1}, 1, 4, 10$. *Note that at* $\hat{t} = 0, 10^{-3}$, *and* 10^{-1} *the subbody is convex and that this convexity, which is not present at* $\hat{t} = 1$, *returns before* $\hat{t} = 4$.

In the experiment under discussion here, the subbodies are congruent and for all $t > t^*$ are star shaped with respect to the midpoints of successive values of x^*. Calculated profiles of a subbody for several times $t = t^* + \hat{t}$ with $\hat{t} > 0$ are seen in Fig. 3. When $\hat{t} = 10$ each component is a sphere in the sense that $\hat{r}(\varphi, t^* + 10)$ is constant in φ to within six significant figures; of course, the collection of spheres so obtained is the new equilibrium state of the original perturbed cylinder.

The initial data for the second numerical experiment correspond to

$$
\begin{aligned}
(5.14) \qquad r_0(x) = 1 &+ 10^{-2}[\sin(2x) + \sin(13x/6) + \sin(7x/3) \\
&+ \sin(5x/2) + \sin(8x/3) + \sin(17x/6)].
\end{aligned}
$$

In this case r_0 has minimum period 12π. For the finite element computation, $b - a$ was chosen to be 12π, i.e., one period. As in the previous case, the interval $a \le x \le b$ was discretized into 512 equal segments, and the time steps Δt were chosen to be 10^{-4} on an interval that contained the times of initial decay, 10^{-2} during the early growth phase and much smaller as t approached t^*. Numerical results are shown in Figs. 4 and 5. Here, again, albeit only wave-numbers k_i that exceed 1 are present in the initial perturbation, and hence the linear theory predicts that $g(t)$ should decay to zero exponentially in t. A second-order perturbation analysis yields the conclusion that new wave-numbers given by $|k_i - k_j|$ will appear and grow. In the present case there are five distinct values of $|k_i - k_j|$ obeying (5.10), namely, 1/6, 1/3, 1/2, 2/3, 5/6. Of these, three, 1/2, 2/3, 5/6, have rates of growth, $\alpha(1/2) = 3/16 = 0.1875$, $\alpha(2/3) = 20/9^2 \simeq 0.2469$, $\alpha(5/6) = 275/36^2 \simeq 0.2122$, that are close to maximum growth rate $\alpha(1/\sqrt{2}) = 0.25$. The periods $2\pi |k_i - k_j|^{-1}$ corresponding to these three fast-growing modes are $4\pi, 3\pi, 12\pi/5$. The distances between adjacent local minima of $r(x, t^*)$ were found to be 9.35115, 9.42478, and 9.57204. One of these values is equal, up to five decimal places, to $3\pi \simeq 9.42478$, and the other two are much nearer to 3π than to either 4π or $12\pi/5$. As $\alpha(1/2)$ and $\alpha(5/6)$ both are less than $\alpha(2/3)$, it is not surprising that an examination of spatial frequencies at $t = t^*$ confirms that the mode with wave-number 2/3 (period 3π) dominates the growth.

Whereas in the first experiment the body breaks into congruent subbodies, in this experiment the break-up at time t^* yields two distinct equivalence classes $\mathcal{C}_1$ and $\mathcal{C}_2$ of congruent bodies. Figure 5d makes this clear. At $t = t^*$, the bodies in $\mathcal{C}_1$ have length 9.57204, and those in $\mathcal{C}_2$ have length $28.12708 = 2 \times 9.33115 + 9.42478$. We have found that members of $\mathcal{C}_1$ remain star shaped for all $t > t^*$, and the spherical-coordinate formulation can be employed to follow their evolution to a final equilibrium state which is spherical. On the other hand, the bodies in $\mathcal{C}_2$ cease to be star shaped at a finite time, and for them the spherical-coordinate formulation is not applicable without major modification. Here the question arises as to whether subbodies of class $\mathcal{C}_2$ will exhibit further break-up or end up as a single sphere. The search for a general algorithm to study post break-up behavior is a topic of current research.
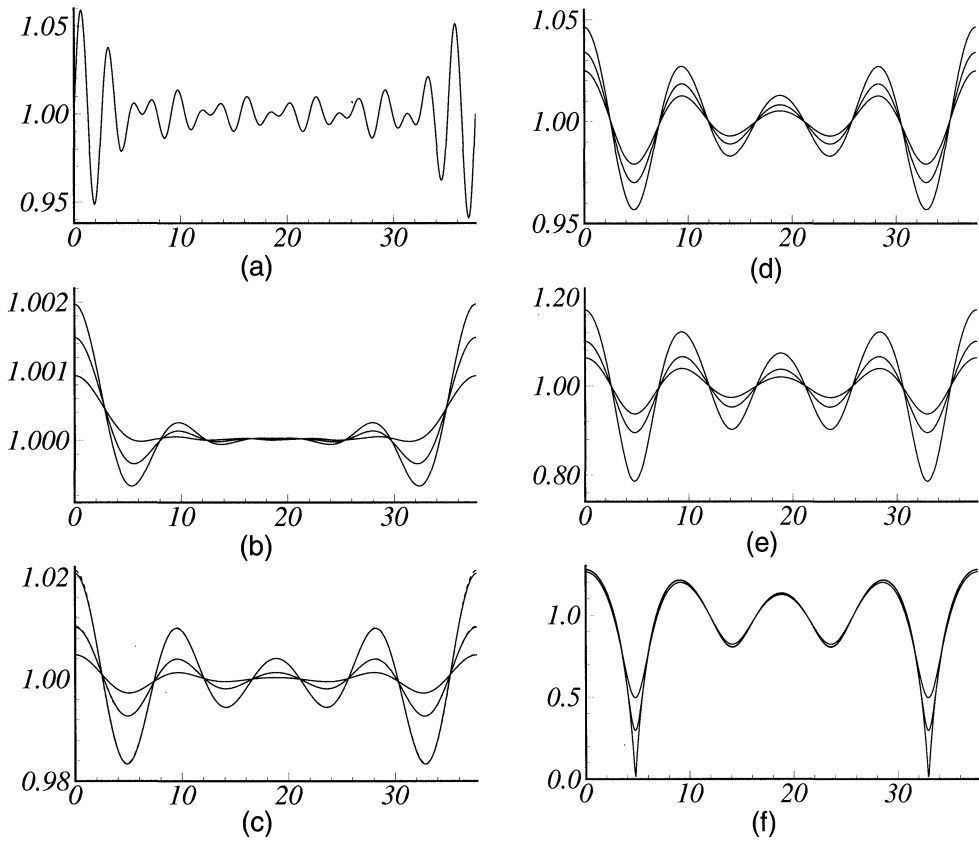
FIG. 4. *The radius r as a function of x in the second numerical experiment*: (a) $t = 0$; (b) $t = 0.7, 4.7, 6.7$; (c) $t = 12, 16, 19$; (d) $t = 20, 22, 24$; (e) $t = 26, 28, 30$; (f) $t = 31.5, 31.7, 31.7357$.
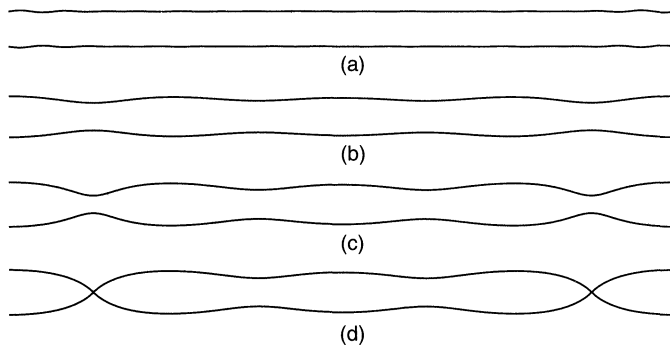

FIG. 5. *Profiles in the second experiment*: (a) $t = 0$; (b) $t = 30$; (c) $t = 31.5$; (d) $t = t^* = 31.7357$.

REFERENCES

[1] J. W. CAHN AND J. E. TAYLOR, *Surface motion by surface diffusion*, Acta Metall. Mater., 42 (1994), pp. 1045–1063.
[2] B. D. COLEMAN, R. S. FALK, AND M. MOAKHER, *Stability of cylindrical bodies in the theory of surface diffusion*, Phy. D, 89 (1995), pp. 123–135.
[3] G. DZIUK, *An algorithm for evolutionary surfaces*, Numer. Math., 58 (1991), pp. 603–611.

[4] C. M. ELLIOTT AND H. GARCKE, *Existence results for diffusive surface motion laws*, preprint.

[5] L. C. EVANS AND J. SPRUCK, *Motion of level sets by mean curvature* I, J. Differential Geom., 33 (1991),
     pp. 635–681.

[6] C. HERRING, *Surface diffusion as a motivation for sintering*, in The Physics of Powder Metallurgy,
     W. E. Kingston, ed., McGraw Hill, New York, 1951, pp. 143–179.

[7] G. HUISKEN, *Flow by mean curvature of convex surfaces into spheres*, J. Differential Geom., 20 (1984),
     pp. 237–266.

[8] ———, *Local and global behaviour of hypersurfaces moving by mean curvature*, in Differential Geometry:
     Partial Differential Equations on Manifolds, R. Greene and S. T. Yau, eds., American Mathematical
     Society, Providence, RI, 1993, pp. 175–191.

[9] W. W. MULLINS, *Theory of thermal grooving*, J. Appl. Phys., 28 (1957), pp. 333–339.

[10] F. A. NICHOLS AND W. W. MULLINS, *Surface- (interface-) and volume-diffusion contribution to morphological
     changes driven by capillarity*, Trans. Metall. Soc., A.I.M.E., 233 (1965), pp. 1840–1847.

[11] J. A. SETHIAN, *Curvature and the evolution of fronts*, Comm. Math. Phys., 101 (1985), pp. 487–499.

[12] H. M. SONER AND P. E. SONGANIDIS, *Singularities and uniqueness of cylindrically symmetric surfaces moving
     by mean curvature*, Comm. Partial Differential Equations, 18 (1993), pp. 859–894.